Chapter 2

Heart rate variability

Heart rate variability (HRV) describes the variations between consecutive heartbeats. The rhythm of the heart is controlled by the *sinoatrial* (SA) node, which is modulated by both the sympathetic and parasympathetic branches of the autonomic nervous system. Sympathetic activity tends to increase heart rate (HR↑) and its response is slow (few seconds) [3]. Parasympathetic activity, on the other hand, tends to decrease heart rate (HR↓) and mediates faster (0.2–0.6 seconds) [3]. In addition to central control, there are some feedback mechanisms that can provide quick reflexes. One such mechanism is the arterial baroreflex. This reflex is based on baroreceptors which are located on the walls of some large vessels and can sense the stretching of vessel walls caused by pressure increase. Both sympathetic and parasympathetic activity are influenced by baroreceptor stimulation trough a specific baroreflex arc, Fig. 2.1.

The continuous modulation of the sympathetic and parasympathetic innervations results in variations in heart rate. The most conspicuous periodic component of HRV is the so-called *respiratory sinus arrhythmia* (RSA) which is considered to range from 0.15 to 0.4 Hz [3]. In addition to the physiological influence of breathing on HRV, this *high frequency* (HF) component is generally believed to be of parasympathetic origin. Another widely studied component of HRV is the *low frequency* (LF) component usually ranging from 0.04 to 0.15 Hz including the component referred to as the 10-second rhythm or the Mayer wave [3]. The rhythms within the LF band have been thought to be of both sympathetic and parasympathetic origin [3] even though some researchers have suggested them to be mainly of sympathetic origin [26]. The fluctuations below 0.04 Hz, on the other hand, have not been studied as much as the higher frequencies. These frequencies are commonly divided into *very low frequency* (VLF, 0.003-0.04 Hz) and *ultra low frequency* (ULF, 0-0.003 Hz) bands, but in case of short-term recordings the ULF band is generally omitted [44]. These lowest frequency rhythms are characteristic for HRV signals and have been related to, e.g., humoral factors such as the thermoregulatory processes and renin-angiotensin system [3].

Even though HRV has been studied extensively during the last decades within which numerous research articles have been published, the practical use of HRV have reached general consensus only in two clinical applications [44]. That is, it can be used as a predictor of risk after myocardial infarction [25, 20] and as an early warning sign of diabetic neuropathy [5, 34]. In addition, HRV has been found to correlate with, e.g., age, mental and physical stress, and attention, see, e.g., the review in [3].

The term HRV refers, in general, to changes in heart beat interval which is a reciprocal of the heart rate. This is also the case here. The starting point for HRV analysis is the ECG recording from which the HRV time series can be extracted. In the formulation of the HRV time series, a fundamental issue is the determination of heart beat period.

2.1 Heart beat period and QRS detection

The aim in HRV analysis is to examine the sinus rhythm modulated by the autonomic nervous system. Therefore, one should technically detect the occurrence times of the SA-node action potentials. This is, however, practically impossible and, thus, the fiducial points for the heart beat is usually determined from the ECG recording. The nearest observable activity in the ECG compared to SA-node firing is the P-wave resulting from atrial depolarization (see Fig. 2.2) and, thus, the heart beat period is generally defined as the time difference between two successive P-waves. The signal-to-noise ratio of the P-wave is, however, clearly lower than that of the strong QRS complex which results primarily from ventricular depolarization. Therefore, the heart beat period is commonly evaluated as the time difference between

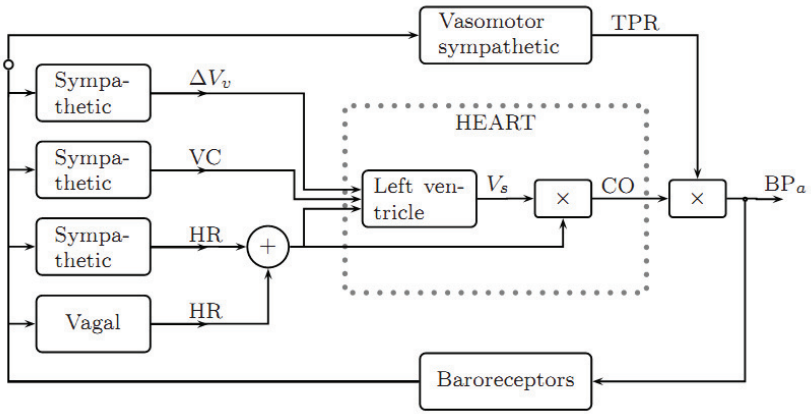

Figure 2.1: The four baroreflex pathways (redrawn from [42]). Variation in venous volume (ΔV_v), left ventricular contractility (VC), sympathetic and parasympathetic (vagal) control of heart rate (HR), stroke volume (V_s), cardiac output (CO), total peripheral resistance (TPR), and arterial blood pressure (BP_a).

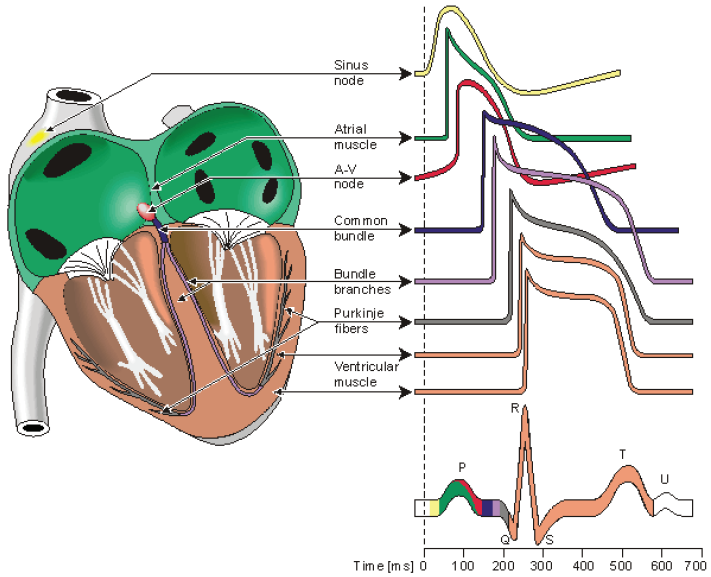

Figure 2.2: Electrophysiology of the heart (redrawn from [27]). The different waveforms for each of the specialized cells found in the heart are shown. The latency shown approximates that normally found in the healthy heart.

the easily detectable QRS complexes.

A typical QRS detector consists of a preprocessing part followed by a decision rule. Several different QRS detectors have been proposed within last decades [45, 35, 36, 18, 13]. For an easy to read review of these methods, see [1]. The preprocessing of the ECG usually includes at least bandpass filtering to reduce power line noise, baseline wander, muscle noise, and other interference components. The passband can be set to approximately 5–30 Hz which covers most of the frequency content of QRS complex [35]. In addition, preprocessing can include differentiation and/or squaring of the samples. After preprocessing, the decision rules are applied to determine whether or not a QRS complex has occurred. The decision rule usually includes an amplitude threshold which is adjusted adaptively as the detection progresses. In addition, the average heart beat period is often used in the decision. The fiducial point is generally selected to be the R-wave and the corresponding time instants are given as the output of the detector.

The accuracy of the R-wave occurrence time estimates is often required to be 1–2 ms and, thus, the sampling frequency of the ECG should be at least 500–1000 Hz [44]. If the sampling frequency of the

ECG is less than 500 Hz, the errors in R-wave occurrence times can cause critical distortion to HRV analysis results, especially to spectrum estimates [31]. The distortion of the spectrum is even bigger if the overall variability in heart rate is small [39]. The estimation accuracy can however be improved by interpolating the QRS complex e.g. by using a cubic spline interpolation [10] or some model based approach [4]. It should be, however, noted that when the SA-node impulses are of interest there is an unavoidable estimation error of approximately 3 ms due to fluctuations in the AV-nodal conduction time [42].

2.2 Derivation of HRV time series

After the QRS complex occurrence times have been estimated, the HRV time series can be derived. The inter-beat intervals or RR intervals are obtained as differences between successive R-wave occurrence times. That is, the n'th RR interval is obtained as the difference between the R-wave occurrence times $\mathrm{RR}_n = t_n - t_{n-1}$. In some context, normal-to-normal (NN) may also be used when referring to these intervals indicating strictly intervals between successive QRS complexes resulting from SA-node depolarization [44]. In practice, the NN and RR intervals appear to be the same and, thus, the term RR is preferred here.

The time series constructed from all available RR intervals is, clearly, not equidistantly sampled, but has to be presented as a function of time, i.e. as values (t_n,RR_n). This fact has to be taken into account before frequency-domain analysis. In general, three different approaches have been used to get around this issue [44]. The simplest approach that have been adopted in, e.g., [2] is to assume equidistant sampling and calculate the spectrum directly from the RR interval tachogram (RR intervals as a function of beat number), see the left panel of Fig. 2.3. This assumption can, however, cause distortion into the spectrum [29]. This distortion becomes substantial when the variability is large in comparison with the mean level. Furthermore, the spectrum can not be considered to be a function of frequency but rather of cycles per beat [11]. Another common approach, adopted in this software, is to use interpolation methods for converting the non-equidistantly sampled RR interval time series (also called the interval function) to equidistantly sampled [44], see the right panel of Fig. 2.3. One choice for the interpolation method is the cubic spline interpolation [29]. After interpolation, regular spectrum estimation methods can be applied. The third general approach called the spectrum of counts considers a series of impulses (delta functions positioned at beat occurrence times) [12]. This approach relies on the generally accepted *integral pulse frequency modulator* (IPFM) which aims to model the neural modulation of the SA-node [42]. According to this model, the modulating signal is integrated until a reference level is achieved after which an impulse is emitted and the integrator is set to zero. The spectrum of the series of events can be calculated, e.g., by first lowpass filtering the event series and then calculating the spectrum of the resulting signal [11].

2.3 Preprocessing of HRV time series

Any artifact in the RR interval time series may interfere the analysis of these signals. The artifacts within HRV signals can be divided into technical and physiological artifacts. The technical artifacts can include missing or additional QRS complex detections and errors in R-wave occurrence times. These artifacts may be due to measurement artifacts or the computational algorithm. The physiological artifacts, on the other hand, include ectopic beats and arrhythmic events. In order to avoid the interference of such artifacts, the ECG recording and the corresponding event series should always be manually checked for artifacts and only artifact-free sections should be included in the analysis [44]. Alternatively, if the amount of artifact-free data is insufficient, proper interpolation methods can be used to reduce these artifacts, see, e.g., [22, 23, 30].

Another common feature that can alter the analysis significantly are the slow linear or more complex trends within the analyzed time series. Such slow nonstationarities are characteristic for HRV signals and should be considered before the analysis. The origins of nonstationarities in HRV are discussed, e.g., in [3]. Two kinds of methods have been used to get around the nonstationarity problem. In [48], it was suggested that HRV data should be systematically tested for nonstationarities and that only stationary segments should be analyzed. Representativeness of these segments in comparison with the whole HRV signal was, however, questioned in [16]. Other methods try to remove the slow nonstationary trends from the HRV signal before analysis. The detrending is usually based on first order [24, 32] or higher order polynomial [40, 32] models. In addition, this software includes an advanced detrending procedure originally presented in [43]. This approach is based on smoothness priors regularization.

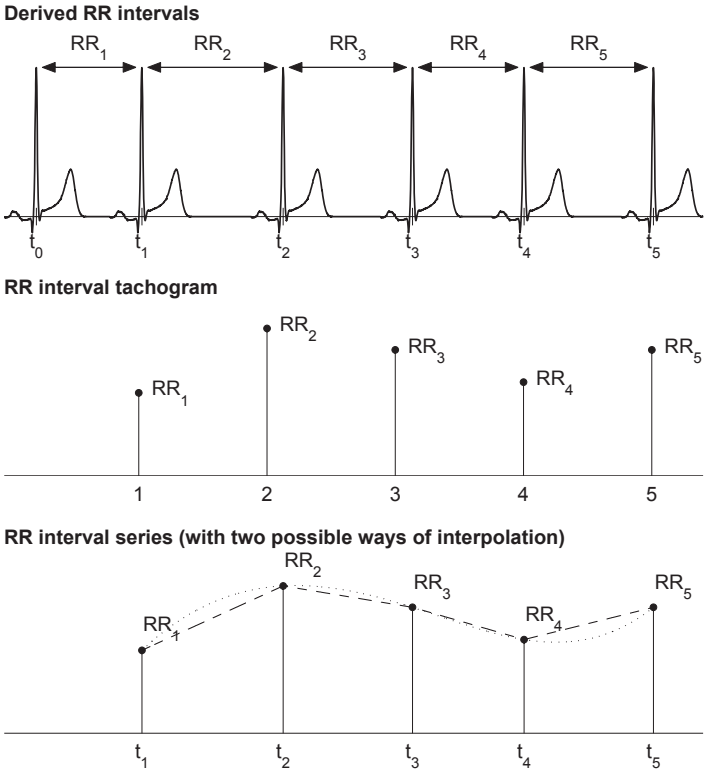

Figure 2.3: Derivation of two HRV signals from ECG: the interval tachogram (middle panel) and interpolated RR interval series (bottom panel).

2.3.1 Smoothness priors based detrending approach

Let $z \in \mathbb{R}^N$ denote the RR interval time series which can be considered to consist of two components

$$z = z_{\text{stat}} + z_{\text{trend}} \tag{2.1}$$

where z_{stat} is the nearly stationary RR interval series of interest, z_{trend} is the low frequency aperiodic trend component, and N is the number of RR intervals. Suppose that the trend component can be modeled with a linear observation model as

$$z_{\text{trend}} = H\theta + e \tag{2.2}$$

where $H \in \mathbb{R}^{N\times p}$ is the observation matrix, $\theta \in \mathbb{R}^p$ are the regression parameters, and e is the observation error. The task is then to estimate the parameters by some fitting procedure so that $\hat{z}_{\text{trend}} = H\hat{\theta}$ can be used as the estimate of the trend. The properties of the estimate depend strongly on the properties of the basis vectors (columns of the matrix H) in the fitting. A widely used method for the solution of the estimate $\hat{\theta}$ is the least squares method. However, a more general approach for the estimation of $\hat{\theta}$ is used here. That is, the so-called regularized least squares solution

$$\hat{\theta}_\lambda = \arg\min_\theta \left\{ \|z - H\theta\|^2 + \lambda^2 \|D_d(H\theta)\|^2 \right\} \tag{2.3}$$

where λ is the regularization parameter and D_d indicates the discrete approximation of the d'th derivative operator. This is clearly a modification of the ordinary least squares solution to the direction in which the side norm $\|D_d(H\theta)\|$ gets smaller. In this way, prior information about the predicted trend $H\theta$ can be implemented to the estimation. The solution of (2.3) can be written in the form

$$\hat{\theta}_\lambda = (H^T H + \lambda^2 H^T D_d^T D_d H)^{-1} H^T z \tag{2.4}$$

and the estimate for the trend which is to be removed as

$$\hat{z}_{\text{trend}} = H\hat{\theta}_\lambda. \tag{2.5}$$

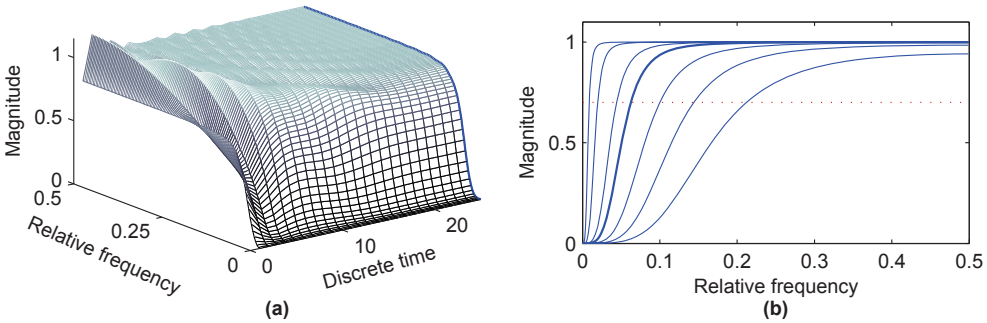

Figure 2.4: a) Time-varying frequency response of $\mathcal{L}$ ($N-1=50$ and $\lambda=10$). Only the first half of the frequency response is presented, since the other half is identical. b) Frequency responses, obtained from the middle row of $\mathcal{L}$ (cf. bold lines), for $\lambda=1$, 2, 4, 10, 20, 100, and 500. The corresponding cut-off frequencies are 0.213, 0.145, 0.101, 0.063, 0.045, 0.021 and 0.010 times the sampling frequency.

The selection of the observation matrix H can be implemented according to some known properties of the data z. For example, a generic set of Gaussian shaped functions or sigmoids can be used. Here, however, the trivial choice of identity matrix $H=I\in\mathbb{R}^{N\times N}$ is used. In this case, the regularization part of (2.3) can be understood to draw the solution towards the null space of the regularization matrix D_d. The null space of the second order difference matrix contains all first order curves and, thus, D_2 is a good choice for estimating the aperiodic trend of RR series. With these specific choices, the detrended nearly stationary RR series can be written as

$$\hat{z}_{\mathrm{stat}}=z-H\hat{\theta}_\lambda=(I-(I+\lambda^2D_2^TD_2)^{-1})z. \tag{2.6}$$

In order to demonstrate the properties of the proposed detrending method, its frequency response is considered. Equation (2.5) can be written as $\hat{z}_{\mathrm{stat}}=\mathcal{L}z$, where $\mathcal{L}=I-(I+\lambda^2D_2^TD_2)^{-1}$ corresponds to a time-varying finite impulse response highpass filter. The frequency response of $\mathcal{L}$ for each discrete time point, obtained as a Fourier transform of its rows, is presented in Fig. 2.4 (a). It can be seen that the filter is mostly constant but the beginning and end of the signal are handled differently. The filtering effect is attenuated for the first and last elements of z and, thus, the distortion of end points of data is avoided. The effect of the smoothing parameter λ on the frequency response of the filter is presented in Fig. 2.4 (b). The cutoff frequency of the filter decreases when λ is increased. Besides the λ parameter the frequency response naturally depends on the sampling rate of signal z.

Chapter 3

Analysis methods

In this chapter, the analysis methods used in the software are introduced. The presented methods are mainly based on the guidelines given in [44]. The presentation of the methods is divided into three categories, i.e. time-domain, frequency-domain and nonlinear methods. The methods summarized in Table 3.1.

3.1 Time-domain methods

The time-domain methods are the simplest to perform since they are applied straight to the series of successive RR interval values. The most evident such measure is the mean value of RR intervals ($\overline{\text{RR}}$) or, correspondingly, the mean HR ($\overline{\text{HR}}$). In addition, several variables that measure the variability within the RR series exist. The standard deviation of RR intervals (SDNN) is defined as

$$\text{SDNN} = \sqrt{\frac{1}{N-1}\sum_{j=1}^{N}(\text{RR}_j - \overline{\text{RR}})^2} \tag{3.1}$$

where RR_j denotes the value of j'th RR interval and N is the total number of successive intervals. The SDNN reflects the overall (both short-term and long-term) variation within the RR interval series, whereas the standard deviation of successive RR interval differences (SDSD) given by

$$\text{SDSD} = \sqrt{E\{\Delta\text{RR}_j^2\} - E\{\Delta\text{RR}_j\}^2} \tag{3.2}$$

can be used as a measure of the short-term variability. For stationary RR series $E\{\Delta\text{RR}_j\} = E\{RR_{j+1}\} - E\{RR_j\} = 0$ and SDSD equals the root mean square of successive differences (RMSSD) given by

$$\text{RMSSD} = \sqrt{\frac{1}{N-1}\sum_{j=1}^{N-1}(\text{RR}_{j+1} - \text{RR}_j)^2}. \tag{3.3}$$

Another measure calculated from successive RR interval differences is the NN50 which is the number of successive intervals differing more than 50 ms or the corresponding relative amount

$$\text{pNN50} = \frac{\text{NN50}}{N-1} \times 100\%. \tag{3.4}$$

In addition to the above statistical measures, there are some geometric measures that are calculated from the RR interval histogram. The HRV triangular index is obtained as the integral of the histogram (i.e. total number of RR intervals) divided by the height of the histogram which depends on the selected bin width. In order to obtain comparable results, a bin width of 1/128 seconds is recommended [44]. Another geometric measure is the TINN which is the baseline width of the RR histogram evaluated through triangular interpolation, see [44] for details.

3.2 Frequency-domain methods

In the frequency-domain methods, a *power spectrum density* (PSD) estimate is calculated for the RR interval series. The regular PSD estimators implicitly assume equidistant sampling and, thus, the RR

interval series is converted to equidistantly sampled series by interpolation methods prior to PSD estimation. In the software a cubic spline interpolation method is used. In HRV analysis, the PSD estimation is generally carried out using either FFT based methods or parametric AR modeling based methods. For details on these methods see, e.g., [28]. The advantage of FFT based methods is the simplicity of implementation, while the AR spectrum yields improved resolution especially for short samples. Another property of AR spectrum that has made it popular in HRV analysis is that it can be factorized into separate spectral components. The disadvantages of the AR spectrum are the complexity of model order selection and the contingency of negative components in the spectral factorization. Nevertheless, it may be advantageous to calculate the spectrum with both methods to have comparable results.

In this software, the HRV spectrum is calculated with FFT based Welch's periodogram method and with the AR method. Spectrum factorization in AR method is optional. In the Welch's periodogram method the HRV sample is divided into overlapping segments. The spectrum is then obtained by averaging the spectra of these segments. This method decreases the variance of the FFT spectrum.

The generalized frequency bands in case of short-term HRV recordings are the very low frequency (VLF, 0–0.04 Hz), low frequency (LF, 0.04–0.15 Hz), and high frequency (HF, 0.15–0.4 Hz). The frequency-domain measures extracted from the PSD estimate for each frequency band include absolute and relative powers of VLF, LF, and HF bands, LF and HF band powers in normalized units, the LF/HF power ratio, and peak frequencies for each band (see Table 3.1). In the case of FFT spectrum, absolute power values for each frequency band are obtained by simply integrating the spectrum over the band limits. In the case of AR spectrum, on the other hand, if factorization is enabled distinct spectral components emerge for each frequency band with a proper selection of the model order and the absolute power values are obtained directly as the powers of these components. If factorization is disabled the AR spectrum powers are calculated as for the FFT spectrum. The band powers in relative and normalized units are obtained from the absolute values as described in Table 3.1.

3.3 Nonlinear methods

Considering the complex control systems of the heart it is reasonable to assume that nonlinear mechanisms are involved in the genesis of HRV. The nonlinear properties of HRV have been analyzed using measures such as Poincaré plot [6, 7], approximate and sample entropy [41, 14], detrended fluctuation analysis [37, 38], correlation dimension [17, 19], and recurrence plots [47, 46, 49]. During the last years, the number of studies utilizing such methods have increased substantially. The downside of these methods is still, however, the difficulty of physiological interpretation of the results.

3.3.1 Poincaré plot

One commonly used nonlinear method that is simple to interpret is the so-called Poincaré plot. It is a graphical representation of the correlation between successive RR intervals, i.e. plot of RR_{j+1} as a function of RR_j as described in Fig. 3.1. The shape of the plot is the essential feature. A common approach to parameterize the shape is to fit an ellipse to the plot as shown in Fig. 3.1. The ellipse is oriented according to the line-of-identity ($\mathrm{RR}_j = \mathrm{RR}_{j+1}$) [6]. The standard deviation of the points perpendicular to the line-of-identity denoted by SD1 describes short-term variability which is mainly caused by RSA. It can be shown that SD1 is related to the time-domain measure SDSD according to [6]

$$\mathrm{SD1}^2 = \frac{1}{2}\mathrm{SDSD}^2. \tag{3.5}$$

The standard deviation along the line-of-identity denoted by SD2, on the other hand, describes long-term variability and has been shown to be related to time-domain measures SDNN and SDSD by [6]

$$\mathrm{SD2}^2 = 2\,\mathrm{SDNN}^2 - \frac{1}{2}\mathrm{SDSD}^2. \tag{3.6}$$

The standard Poincaré plot can be considered to be of the first order. The second order plot would be a three dimensional plot of values $(\mathrm{RR}_j, \mathrm{RR}_{j+1}, \mathrm{RR}_{j+2})$. In addition, the lag can be bigger than 1, e.g., the plot $(\mathrm{RR}_j, \mathrm{RR}_{j+2})$.

3.3.2 Approximate entropy

Approximate entropy (ApEn) measures the complexity or irregularity of the signal [14, 41]. Large values of ApEn indicate high irregularity and smaller values of ApEn more regular signal. The ApEn is computed

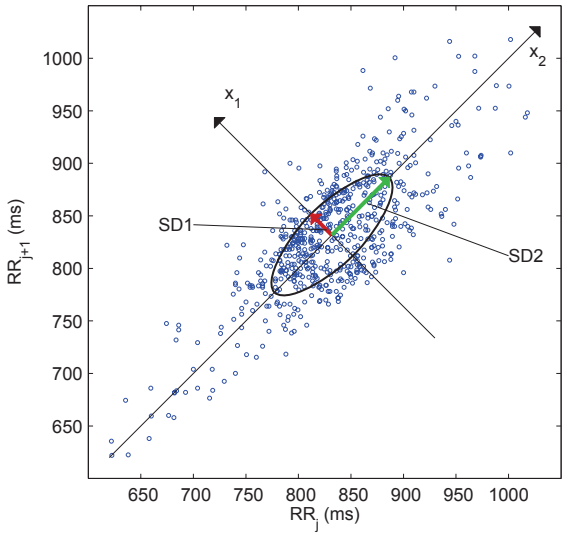

Figure 3.1: Poincaré plot analysis with the ellipse fitting procedure. SD1 and SD2 are the standard deviations in the directions x_1 and x_2, where x_2 is the line-of-identity for which $\mathrm{RR}_j = \mathrm{RR}_{j+1}$.

as follows.

First, a set of length m vectors u_j is formed

$$u_j = (\mathrm{RR}_j, \mathrm{RR}_{j+1}, \ldots, \mathrm{RR}_{j+m-1}), \quad j = 1, 2, \ldots N - m + 1 \tag{3.7}$$

where m is called the embedding dimension and N is the number of measured RR intervals. The distance between these vectors is defined as the maximum absolute difference between the corresponding elements, i.e.,

$$d(u_j, u_k) = \max\left\{ |\mathrm{RR}_{j+n} - \mathrm{RR}_{k+n}| \,\middle|\, n = 0, \ldots, m-1 \right\}. \tag{3.8}$$

Next, for each u_j the relative number of vectors u_k for which $d(u_j, u_k) \leq r$ is calculated. This index is denoted with $C_j^m(r)$ and can be written in the form

$$C_j^m(r) = \frac{\text{nbr of } \left\{ u_k \,\middle|\, d(u_j, u_k) \leq r \right\}}{N - m + 1} \quad \forall\, k. \tag{3.9}$$

Due to the normalization, the value of $C_j^m(r)$ is always smaller or equal to 1. Note that the value is, however, at least $1/(N - m + 1)$ since u_j is also included in the count. Then, take the natural logarithm of each $C_j^m(r)$ and average over j to yield

$$\Phi^m(r) = \frac{1}{N - m + 1} \sum_{j=1}^{N-m+1} \ln C_j^m(r). \tag{3.10}$$

Finally, the approximate entropy is obtained as

$$\mathrm{ApEn}(m, r, N) = \Phi^m(r) - \Phi^{m+1}(r). \tag{3.11}$$

Thus, the value of the estimate ApEn depends on three parameters, the length m of the vectors u_j, the tolerance value r, and the data length N. In this software the default value of m is set to be $m = 2$. The length N of the data also affects ApEn. When N is increased the ApEn approaches its asymptotic value. The tolerance r has a strong effect on ApEn and it should be selected as a fraction of the standard deviation of the data (SDNN). This selection enables the comparison of different data types. A common selection for r is $r = 0.2SDNN$, which is also the default value in this software.

3.3.3 Sample entropy

Sample entropy (SampEn) is similar to ApEn, but there are two important differences in its calculation [41, 21]. For ApEn, in the calculation of the number of vectors u_k for which $d(u_j, u_k) \leq r$ also the

vector u_j itself is included. This ensures that $C_j^m(r)$ is always larger than 0 and the logarithm can be applied, but at the same time it makes ApEn to be biased. In sample entropy the self-comparison of u_j is eliminated by calculating $C_j^m(r)$ as

$$C_j^m(r) = \frac{\text{nbr of } \left\{u_k \,\middle|\, d(u_j, u_k) \leq r\right\}}{N-m} \quad \forall\, k \neq j. \tag{3.12}$$

Now the value of $C_j^m(r)$ will be between 0 and 1. Next, the values of $C_j^m(r)$ are averaged to yield

$$C^m(r) = \frac{1}{N-m+1} \sum_{j=1}^{N-m+1} C_j^m(r) \tag{3.13}$$

and the sample entropy is obtained as

$$\text{SampEn}(m, r, N) = \ln\left(C^m(r)/C^{m+1}(r)\right). \tag{3.14}$$

The default values set for the embedding dimension m and for the tolerance parameter r in the software are the same as those for the approximate entropy calculation. Both ApEn and SampEn are estimates for the negative natural logarithm of the conditional probability that a data of length N, having repeated itself within a tolerance r for m points, will also repeat itself for $m+1$ points. SampEn was designed to reduce the bias of ApEn and has a closer agreement with the theory for data with known probabilistic content [21].

3.3.4 Multiscale entropy (MSE)

Multiscale entropy (MSE) is an extension of SampEn in the sense that it incorporates two procedures [8]

1. A *course-graining* process is applied to the RR interval time series. Multiple course-grained time series are constructed for the time series by averaging the data points within non-overlapping windows of increasing length τ, where τ represents the scale factor and is selected to range between $\tau = 1, 2, \ldots, 20$. The length of each course-grained time series is N/τ, where N is the number of RR intervals in the data. For scale $\tau = 1$, the course-grained time series is simply the original beat-to-beat RR interval time series.

2. SampEn is calculated for each course-grained time series. SampEn as a function of the scale factor produces the MSE. MSE for scale factor $\tau = 1$ returns standard SampEn (computed from the original data points).

3.3.5 Detrended fluctuation analysis

Detrended fluctuation analysis (DFA) measures the correlation within the signal. The correlation is extracted for different time scales as follows [37]. First, the RR interval time series is integrated

$$y(k) = \sum_{j=1}^{k} (\text{RR}_j - \overline{\text{RR}}), \quad k = 1, \ldots, N \tag{3.15}$$

where $\overline{\text{RR}}$ is the average RR interval. Next, the integrated series is divided into segments of equal length n. Within each segment, a least squares line is fitted into the data. Let $y_n(k)$ denote these regression lines. Next the integrated series $y(k)$ is detrended by subtracting the local trend within each segment and the root-mean-square fluctuation of this integrated and detrended time series is calculated by

$$F(n) = \sqrt{\frac{1}{N} \sum_{k=1}^{N} (y(k) - y_n(k))^2}. \tag{3.16}$$

This computation is repeated over different segment lengths to yield the index $F(n)$ as a function of segment length n. Typically $F(n)$ increases with segment length. A linear relationship on a double log graph indicates presence of fractal scaling and the fluctuations can be characterized by scaling exponent α (the slope of the regression line relating $\log F(n)$ to $\log n$. Different values of α indicate the following

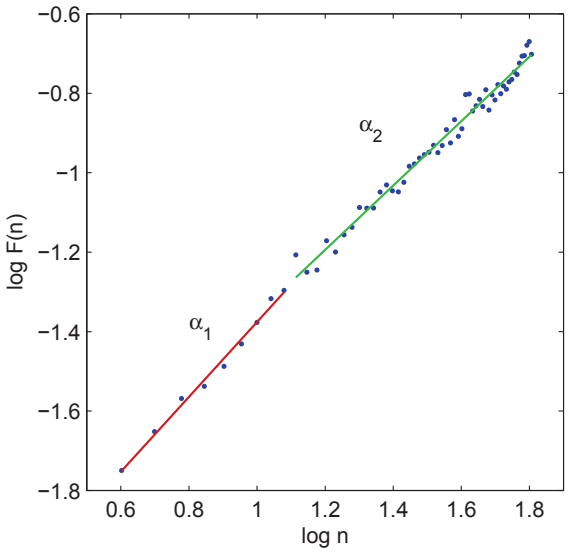

Figure 3.2: Detrended fluctuation analysis. A double log plot of the index $F(n)$ as a function of segment length n. α_1 and α_2 are the short term and long term fluctuation slopes, respectively.

$\alpha = 1.5$:	Brown noise (integral of white noise)
$1 < \alpha < 1.5$:	Different kinds of noise
$\alpha = 1$:	$1/f$ noise
$0.5 < \alpha < 1$:	Large values are likely to be followed by large value and vice versa
$\alpha = 0.5$:	white noise
$0 < \alpha < 0.5$:	Large value is likely to be followed by small value and vice versa

Typically, in DFA the correlations are divided into short-term and long-term fluctuations. In the software, the short-term fluctuations are characterized by the slope α_1 obtained from the ($\log n$,$\log F(n)$) graph within range $4 \leq n \leq 16$ (default values). Correspondingly, the slope α_2 obtained by default from the range $16 \leq n \leq 64$ characterizes long-term fluctuations, see Fig. 3.2.

3.3.6 Correlation dimension

Another method for measuring the complexity or strangeness of the time series is the correlation dimension which was proposed in [15]. The correlation dimension is expected to give information on the minimum number of dynamic variables needed to model the underlying system and it can be obtained as follows.

Similarly as in the calculation of approximate and sample entropies, form length m vectors u_j

$$u_j = (\mathrm{RR}_j, \mathrm{RR}_{j+1}, \ldots, \mathrm{RR}_{j+m-1}), \quad j = 1, 2, \ldots, N-m+1 \tag{3.17}$$

and calculate the number of vectors u_k for which $d(u_j, u_k) \leq r$, that is

$$C_j^m(r) = \frac{\text{nbr of } \left\{u_k \,\middle|\, d(u_j, u_k) \leq r\right\}}{N-m+1} \quad \forall\, k \tag{3.18}$$

where the distance function $d(u_j, u_k)$ is now defined as

$$d(u_j, u_k) = \sqrt{\sum_{l=1}^{m} (u_j(l) - u_k(l))^2}. \tag{3.19}$$

Next, an average of the term $C_j^m(r)$ is taken

$$C^m(r) = \frac{1}{N-m+1} \sum_{j=1}^{N-m+1} C_j^m(r) \tag{3.20}$$

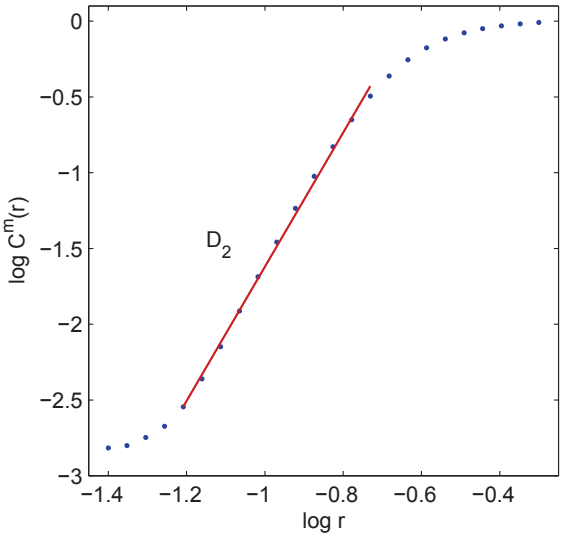

Figure 3.3: Approximation of the correlation dimension D_2 from the $(\log r, \log C^m(r))$ plot.

which is the so-called correlation integral. The correlation dimension D_2 is defined as the limit value

$$D_2(m) = \lim_{r\to 0} \lim_{N\to\infty} \frac{\log C^m(r)}{\log r}. \tag{3.21}$$

In practice this limit value is approximated by the slope of the regression curve $(\log r, \log C^m(r))$ [19]. The slope is calculated from the linear part of the log-log plot, see Fig. 3.3. The slope of the regression curves tend to saturate on the finite value of D_2 when m is increased. In the software, a default value of $m = 10$ was selected for the embedding.

3.3.7 Recurrence plot analysis

Yet another approach, included in the software, for analyzing the complexity of the time series is the so-called *recurrence plot* (RP) analysis. In this approach, vectors

$$u_j = (\mathrm{RR}_j, \mathrm{RR}_{j+\tau}, \ldots, \mathrm{RR}_{j+(m-1)\tau}), \quad j = 1, 2, \ldots, N-(m-1)\tau \tag{3.22}$$

where m is the embedding dimension and τ the embedding lag. The vectors u_j then represent the RR interval time series as a trajectory in m dimensional space. A recurrence plot is a symmetrical $[N-(m-1)\tau] \times [N-(m-1)\tau]$ matrix of zeros and ones. The element in the j'th row and k'th column of the RP matrix, i.e. RP(j,k), is 1 if the point u_j on the trajectory is close to point u_k. That is

$$\mathrm{RP}(j,k) = \begin{cases} 1, & d(u_j - u_k) \le r \\ 0, & \text{otherwise} \end{cases} \tag{3.23}$$

where $d(u_j, u_k)$ is the Euclidean distance given in (3.19) and r is a fixed threshold. The structure of the RP matrix usually shows short line segments of ones parallel to the main diagonal. The lengths of these diagonal lines describe the duration of which the two points are close to each other. An example RP for HRV time series is presented in Fig. 3.4. Methods for quantifying recurrence plots were proposed in [47]. The methods included in this software are introduced below.

In the software the following selections were made. The embedding dimension and lag were selected to be $m = 10$ (default value) and $\tau = 1$ (fixed), respectively. The threshold distance r was selected to be $\sqrt{m}\,\mathrm{SD}$ (default value), where SD is the standard deviation of the RR time series. The selection are similar to those made in [9].

The first quantitative measure of RP is the *recurrence rate* (REC) which is simply the ratio of ones and zeros in the RP matrix. The number of elements in the RP matrix for $\tau = 1$ is equal to $N - m + 1$ and the recurrence rate is simply given as

$$\mathrm{REC} = \frac{1}{(N-m+1)^2} \sum_{j,k=1}^{N-m+1} \mathrm{RP}(j,k). \tag{3.24}$$

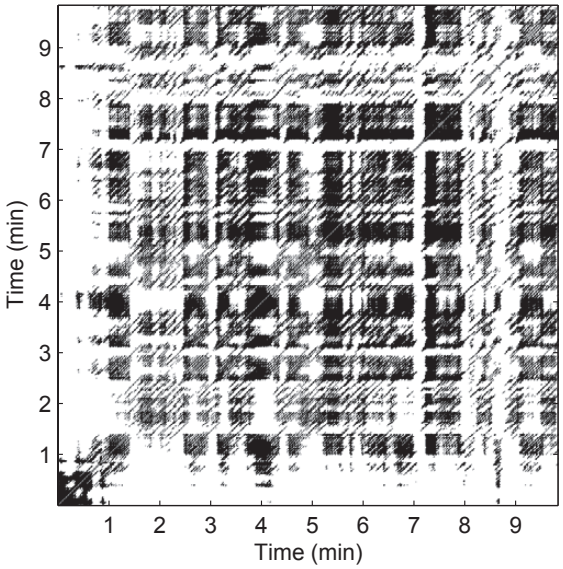

Figure 3.4: Recurrence plot matrix for HRV time series (black = 1 and white = 0).

The recurrence rate can also be calculated separately for each diagonal parallel to the line-of-identity (main diagonal). The trend of REC as a function of the time distance between these diagonals and the line-of-identity describes the fading of the recurrences for points further away.

The rest of the RP measures consider the lengths of the diagonal lines. A threshold $l_{\min} = 2$ is used for excluding the diagonal lines formed by tangential motion of the trajectory. The maximum line length is denoted $l_{\max}$ and its inverse, the divergence,

$$\mathrm{DIV} = \frac{1}{l_{\max}} \tag{3.25}$$

has been shown to correlate with the largest positive Lyapunov exponent [46]. The average diagonal line length, on the other hand, is obtained as

$$l_{\mathrm{mean}} = \frac{\sum_{l=l_{\min}}^{l_{\max}} l N_l}{\sum_{l=l_{\min}}^{l_{\max}} N_l} \tag{3.26}$$

where N_l is the number of length l lines. The determinism of the time series is measured by the variable

$$\mathrm{DET} = \frac{\sum_{l=l_{\min}}^{l_{\max}} l N_l}{\sum_{j,k=1}^{N-m+1} \mathrm{RP}(j,k)}. \tag{3.27}$$

Finally, the Shannon information entropy of the line length distribution is defined as

$$\mathrm{ShanEn} = -\sum_{l=l_{\min}}^{l_{\max}} n_l \ln n_l \tag{3.28}$$

where n_l is the number of length l lines divided by the total number of lines, that is

$$n_l = \frac{N_l}{\sum_{l'=l_{\min}}^{l_{\max}} N_{l'}}. \tag{3.29}$$

3.4 Summary of HRV parameters

The presented time-domain, frequency-domain and nonlinear measures of HRV calculated by the software are summarized in Table 3.1. For each measure, preferred units and a short description is given. In addition, a reference to the equation in which the specific measure is defined is given when possible and related references are given for some of the measures.

Table 3.1: Summary of the HRV measures calculated by the software

	Measure	Units	Description	References
Time-Domain	$\overline{RR}$	[ms]	The mean of RR intervals	
	STD RR (SDNN)	[ms]	Standard deviation of RR intervals [Eq. (3.1)]	
	$\overline{HR}$	[1/min]	The mean heart rate	
	STD HR	[1/min]	Standard deviation of intantaneous heart rate values	
	RMSSD	[ms]	Square root of the mean squared differences between successive RR intervals [Eq. (3.3)]	
	NN50		Number of successive RR interval pairs that differ more than 50 ms	
	pNN50	[%]	NN50 divided by the total number of RR intervals [Eq. (3.4)]	
	HRV triangular index		The integral of the RR interval histogram divided by the height of the histogram [44]	
	TINN	[ms]	Baseline width of the RR interval histogram	[44]
Frequency-Domain	Peak frequency	[Hz]	VLF, LF, and HF band peak frequencies	
	Absolute power	[ms^2]	Absolute powers of VLF, LF, and HF bands	
	Relative power	[%]	Relative powers of VLF, LF, and HF bands VLF [%] = VLF [ms^2]/total power [ms^2] $\times$ 100% LF [%] = LF [ms^2]/total power [ms^2] $\times$ 100% HF [%] = HF [ms^2]/total power [ms^2] $\times$ 100%	
	Normalized power	[n.u.]	Powers of LF and HF bands in normalized units LF [n.u.] = LF [ms^2]/(total power [ms^2] $-$ VLF [ms^2]) HF [n.u.] = HF [ms^2]/(total power [ms^2] $-$ VLF [ms^2])	
	LF/HF		Ratio between LF and HF band powers	
Nonlinear	SD1, SD2	[ms]	The standard deviation of the Poincaré plot perpendicular to (SD1) and along (SD2) the line-of-identity	[6, 7]
	ApEn		Approximate entropy [Eq. (3.11)]	[41, 14]
	SampEn		Sample entropy [Eq. (3.14)]	[41]
	D_2		Correlation dimension [Eq. (3.21)]	[17, 19]
	DFA		Detrended fluctuation analysis:	[37, 38]
	α_1		Short term fluctuation slope	
	α_2		Long term fluctuation slope	
	RPA		Recurrence plot analysis:	[47, 9, 49]
	Lmean	[beats]	Mean line length [Eq. (3.26)]	
	Lmax	[beats]	Maximum line length	
	REC	[%]	Recurrence rate [Eq. (3.24)]	
	DET	[%]	Determinism [Eq. (3.27)]	
	ShanEn		Shannon entropy [Eq. (3.28)]	

References

[1] V.X. Afonso. ECG QRS detection. In W.J. Tompkins, editor, *Biomedical Digital Signal Processing*, chapter 12, pages 237–264. Prentice Hall, New Jersey, 1993.

[2] G. Baselli, S. Cerutti, S. Civardi, F. Lombardi, A. Malliani, M. Merri, M. Pagani, and G. Rizzo. Heart rate variability signal processing: a quantitative approach as an aid to diagnosis in cardiovascular pathologies. *Int J Bio-Med Comput*, 20:51–70, 1987.

[3] G.G. Berntson, J.T. Bigger Jr., D.L. Eckberg, P. Grossman, P.G. Kaufmann, M. Malik, H.N. Nagaraja, S.W. Porges, J.P. Saul, P.H. Stone, and M.W. Van Der Molen. Heart rate variability: Origins, methods, and interpretive caveats. *Psychophysiol*, 34:623–648, 1997.

[4] T. Bragge, M. P. Tarvainen, P. O. Ranta-aho, and P. A. Karjalainen. High-resolution QRS fiducial point corrections in sparsely sampled ECG recordings. *Physiol Meas*, 26(5):743–751, 2005.

[5] H.-J. Braune and U. Geisenörfer. Measurement of heart rate variations: influencing factors, normal values and diagnostic impact on diabetic autonomic neuropathy. *Diabetes Res Clin Practice*, 29:179–187, 1995.

[6] M. Brennan, M. Palaniswami, and P. Kamen. Do existing measures of Poincaré plot geometry reflect nonlinear features of heart rate variability. *IEEE Trans Biomed Eng*, 48(11):1342–1347, November 2001.

[7] S. Carrasco, M.J. Caitán, R. González, and O. Yánez. Correlation among Poincaré plot indexes and time and frequency domain measures of heart rate variability. *J Med Eng Technol*, 25(6):240–248, November/December 2001.

[8] M. Costa, A.L. Goldberger, and C.-K. Peng. Multiscale entropy analysis of biological signals. *Physical Rev E*, 71:021906, 2005.

[9] H. Dabire, D. Mestivier, J. Jarnet, M.E. Safar, and N. Phong Chau. Quantification of sympathetic and parasympathetic tones by nonlinear indexes in normotensive rats. *amj*, 44:H1290–H1297, 1998.

[10] I. Daskalov and I. Christov. Improvement of resolution in measurement of electrocardiogram RR intervals by interpolation. *Med Eng Phys*, 19(4):375–379, June 1997.

[11] R.W. DeBoer, J.M. Karemaker, and J. Strackee. Comparing spectra of a series of point events particularly for heart rate variability data. *IEEE Trans Biomed Eng*, 31(4):384–387, April 1984.

[12] R.W. DeBoer, J.M. Karemaker, and J. Strackee. Spectrum of a series of point events, generated by the integral pulse frequency modulation model. *Med Biol Eng Comput*, 23:138–142, March 1985.

[13] G.M. Friesen, T.C. Jannett, M.A. Jadallah, S.L. Yates, S.R. Quint, and H.T. Nagle. A comparison of the noise sensitivity of nine QRS detection algorithms. *IEEE Trans Biomed Eng*, 37(1):85–98, January 1990.

[14] Y. Fusheng, H. Bo, and T. Qingyu. Approximate entropy and its application in biosignal analysis. In M. Akay, editor, *Nonlinear Biomedical Signal Processing: Dynamic Analysis and Modeling*, volume II, chapter 3, pages 72–91. IEEE Press, New York, 2001.

[15] P. Grassberger and I. Procaccia. Characterization of strange attractors. *Phys Rev Lett*, 50:346–349, 1983.

[16] P. Grossman. Breathing rhythms of the heart in a world of no steady state: a comment on Weber, Molenaar, and van der Molen. *Psychophysiol*, 29(1):66–72, January 1992.

[17] S. Guzzetti, M.G. Signorini, C. Cogliati, S. Mezzetti, A. Porta, S. Cerutti, and A. Malliani. Non-linear dynamics and chaotic indices in heart rate variability of normal subjects and heart-transplanted patients. *Cardiovascular Research*, 31:441–446, 1996.

[18] P.S. Hamilton and W.J. Tompkins. Quantitative investigation of QRS detection rules using the MIT/BIH arrhythmia database. *IEEE Trans Biomed Eng*, 33(12):1157–1165, December 1986.

[19] B. Henry, N. Lovell, and F. Camacho. Nonlinear dynamics time series analysis. In M. Akay, editor, *Nonlinear Biomedical Signal Processing: Dynamic Analysis and Modeling*, volume II, chapter 1, pages 1–39. IEEE Press, New York, 2001.

[20] H.V. Huikuri, T.H. Mäkikallio, P. Raatikainen, J. Perkiömäki, A. Castellanos, and R.J. Myerburg. Prediction of sudden cardiac death: appraisal of the studies and methods assessing the risk of sudden arrhythmic death. *Circulation*, 108(1):110–115, July 2003.

[21] D.E. Lake, J.S. Richman, M.P. Griffin, and J.R. Moorman. Sample entropy analysis of neonatal heart rate variability. *ajp*, 283:R789–R797, September 2002.

[22] N. Lippman, K.M. Stein, and B.B. Lerman. Nonlinear predictive interpolation: a new method for the correction of ectopic beats for heart rate variability analysis. *J Electrocardiol*, 26:S14–S19, 1993.

[23] N. Lippman, K.M. Stein, and B.B. Lerman. Comparison of methods for removal of ectopy in measurement of heart rate variability. *Am J Physiol*, 267(1):H411–H418, July 1994.

[24] D.A. Litvack, T.F. Oberlander, L.H. Carney, and J.P. Saul. Time and frequency domain methods for heart rate variability analysis: a methodological comparison. *Psychophysiol*, 32:492–504, 1995.

[25] F. Lombardi, T.H. Mäkikallio, R.J. Myerburg, and H. Huikuri. Sudden cardiac death: role of heart rate variability to identify patients at risk. *Cardiovasc Res*, 50:210–217, 2001.

[26] A. Malliani, M. Pagani, F. Lombardi, and S. Cerutti. Cardiovascular neural regulation explored in the frequency domain. *Circulation*, 84(2):482–492, August 1991.

[27] J. Malmivuo and R. Plonsey. *Bioelectromagnetism: Principles and Applications of Bioelectric and Biomagnetic Fields*. Oxford University Press (Web Edition), 1995.

[28] S.L. Marple. *Digital Spectral Analysis*. Prentice-Hall International, 1987.

[29] J. Mateo and P. Laguna. Improved heart rate variability signal analysis from the beat occurrence times according to the IPFM model. *IEEE Trans Biomed Eng*, 47(8):985–996, August 2000.

[30] J. Mateo and P. Laguna. Analysis of heart rate variability in the presence of ectopic beats using the heart timing signal. *IEEE Trans Biomed Eng*, 50(3):334–343, March 2003.

[31] M. Merri, D.C. Farden, J.G. Mottley, and E.L. Titlebaum. Sampling frequency of the electrocardiogram for spectral analysis of the heart rate variability. *IEEE Trans Biomed Eng*, 37(1):99–106, January 1990.

[32] I.P. Mitov. A method for assessment and processing of biomedical signals containing trend and periodic components. *Med Eng Phys*, 20(9):660–668, November-December 1998.

[33] J-P. Niskanen, M. P. Tarvainen, P. O. Ranta-aho, and P. A. Karjalainen. Software for advanced HRV analysis. *Comput Meth Programs Biomed*, 76(1):73–81, 2004.

[34] M. Pagani. Heart rate variability and autonomic diabetic neuropathy. *Diabetes Nutrition & Metabolism*, 13(6):341–346, 2000.

[35] O. Pahlm and L. Sörnmo. Software QRS detection in ambulatory monitoring – a review. *Med Biol Eng Comput*, 22:289–297, July 1984.

[36] J. Pan and W.J. Tompkins. A real-time QRS detection algorithm. *IEEE Trans Biomed Eng*, 32(3):230–236, March 1985.

[37] C.-K. Peng, S. Havlin, H.E. Stanley, and A.L. Goldberger. Quantification of scaling exponents and crossover phenomena in nonstationary heartbeat time series. *Chaos*, 5:82–87, 1995.

[38] T. Penzel, J.W. Kantelhardt, L. Grote, J.-H. Peter, and A. Bunde. Comparison of detrended fluctuation analysis and spectral analysis for heart rate variability in sleep and sleep apnea. *IEEE Trans Biomed Eng*, 50(10):1143–1151, October 2003.

[39] G.D. Pinna, R. Maestri, A. Di Cesare, R. Colombo, and G. Minuco. The accuracy of power-spectrum analysis of heart-rate variability from annotated RR lists generated by Holter systems. *Physiol Meas*, 15:163–179, 1994.

[40] S.W. Porges and R.E. Bohrer. The analysis of periodic processes in psychophysiological research. In J.T. Cacioppo and L.G. Tassinary, editors, *Principles of Psychophysiology: Physical Social and Inferential Elements*, pages 708–753. Cambridge University Press, 1990.

[41] J.A. Richman and J.R. Moorman. Physiological time-series analysis using approximate entropy and sample entropy. *Am J Physiol*, 278:H2039–H2049, 2000.

[42] O. Rompelman. Rhythms and analysis techniques. In J. Strackee and N. Westerhof, editors, *The Physics of Heart and Circulation*, pages 101–120. Institute of Physics Publishing, Bristol, 1993.

[43] M. P. Tarvainen, P. O. Ranta-aho, and P. A. Karjalainen. An advanced detrending method with application to HRV analysis. *IEEE Trans Biomed Eng*, 49(2):172–175, February 2002.

[44] Task force of the European society of cardiology and the North American society of pacing and electrophysiology. Heart rate variability – standards of measurement, physiological interpretation, and clinical use. *Circulation*, 93(5):1043–1065, March 1996.

[45] N.V. Thakor, J.G. Webster, and W.J. Tompkins. Optimal QRS detector. *Med Biol Eng Comput*, 21:343–350, May 1983.

[46] L.L. Trulla, A. Giuliani, J.P. Zbilut, and C.L. Webber Jr. Recurrence quantification analysis of the logistic equation with transients. *Phys Lett A*, 223(4):255–260, 1996.

[47] C.L. Webber Jr. and J.P. Zbilut. Dynamical assessment of physiological systems and states using recurrence plot strategies. *J Appl Physiol*, 76:965–973, 1994.

[48] E.J.M. Weber, C.M. Molenaar, and M.W. van der Molen. A nonstationarity test for the spectral analysis of physiological time series with an application to respiratory sinus arrhythmia. *Psychophysiol*, 29(1):55–65, January 1992.

[49] J.P. Zbilut, N. Thomasson, and C.L. Webber. Recurrence quantification analysis as a tool for the nonlinear exploration of nonstationary cardiac signals. *Med Eng Phys*, 24:53–60, 2002.